

# APPLICATION OF DIGITAL PHOTOGRAMMETRY IN GEOTECHNICS

R. Roncella<sup>a</sup>, M. Scaioni<sup>b</sup>, G. Forlani<sup>a</sup>

<sup>a</sup> DICATA, Dept. of Civil Engineering, Parma University, Parma, 43100, Italy - (rroncell, gianfranco.forlani)@unipr.it

<sup>b</sup> DIAR, Politecnico of Milan, Milan, 20133, Italy - marco.scaioni@polimi.it

## Commission V, WG 1

**KEY WORDS:** Geology, Engineering, Close Range, Digital, Photogrammetry

### ABSTRACT:

Acquiring geometric data, such as coordinates, displacements or deformations, has always been a way to verify mathematical modelling in civil engineering. The introduction of finite elements methods further reinforced this trend. This paper reports on two applications of photogrammetry to soil and rock mechanics in order to provide an accurate and dense description of the deformation fields of sand specimens in different loading conditions. In the first case, the displacements induced by a foundation under load in sand layers are traced until the collapse of the terrain with accuracies in the order of about 20 micrometers in object space. In the latter, the trajectories of particles, tied to a sloping sand specimen that slides along a plane, are determined with an accuracy of about 3 mm at a rate of 22 fps. In both examples, the measurement runs automatically, the only interaction required being the test setup.

## 1. INTRODUCTION

There is a wide range of tasks in university laboratories where digital photogrammetry is proving to be an ideal measurement tool, from tracing the slow progress of deformations of a specimen in a loading machine to particle tracking in fluids. Requirements in terms of accuracy, measurement rate, number of targets to be tracked and object size are very specific to the applications, so design and setup must be tailored to the specifications of each experiment. Besides often representing interesting tasks in themselves, they also offer the opportunity for interdisciplinary cooperation among different fields, leading to a larger acceptance of photogrammetry within academia. This paper reports on two such experiences, jointly held at the Politecnico of Milan and at the University of Parma, where photogrammetry has been used to support research activities in soil mechanics.

The first had the objective of determining the deformation field induced by the foundations of buildings or bridges in sand layers. This should ultimately lead to improved design techniques of foundations, thanks to the deeper understanding of their interaction with sand. The movement of the sand particles under test were in the order of 100 micrometers at each loading step, so the key point was to follow accurately a very small and slow movement.

In a second application, the goal was to track the movement of the superficial layer of a terrain slope sliding over a discontinuity plane (reproducing at a smaller scale an artificially induced landslide of incoherent soil); again this was meant to verify the prediction of the movement by a mathematical model. In this case, the accuracy requirements were less demanding in absolute terms (1-2 mm) but the dynamics of the movement was significant and the displacement field 3D.

## 2. MEASUREMENT OF DISPLACEMENTS INDUCED BY FOUNDATIONS ON SAND

### 2.1 Background

Evaluation of the tensile strength of a sandy terrain subject to different loading conditions relied so far on methods based on

the elastic model. In reality, this assumption is not completely satisfied, also when dealing with reduced load and small deformations. Since a more accurate knowledge of the maximum load sustainable by a terrain would result in the optimization of foundations design, several experimental tests have been set up at the Dept. of Structural Engineering (D.I.S.) of the Politecnico of Milan to assess the dependency of the mechanical behaviour of the terrain on frequency and magnitude of load cycles as well as on foundation stress. Results of this study will help to prevent situation of risk in case of structures stressed by earthquakes, winds and waves, such as those experienced in off-shore platforms and structures for sea-side protection built over incoherent sand.

### 2.2 Experimental setup

At the Dept. of Structural Engineering, a testing device designed and built to execute load tests on sand specimens has been in use for the last 15 years with several kind of materials and loading configurations (Montrasio & Nova, 1989). As shown in Figure 1, the device is a box (with dimensions 890x20x385 mm) made up of two tempered glass walls, reinforced by steel bars, and two lateral wooden walls. The sand specimen is deposited in the box through a specially designed sieve, so that the stratification and density of real terrain can be reproduced. The scale model of foundation press the sand, just fitting the size of the device but without direct contact with the lateral glass walls, to avoid friction. Thanks to a pair of oleodynamic actuators, loads in horizontal and vertical direction may be applied, while two strain-gauges along the same directions perform a continuous measurement of displacements. Cyclic loading is possible as well. The typical outcome from this instrument is the diagram load-displacement for the point located just below the foundation centre. Until photogrammetry was used, no quantitative evaluation about the displacements at any other location of the terrain underneath could be derived. A qualitative information was obtained by inserting coloured horizontal sandy layers and taking some pictures during trials.

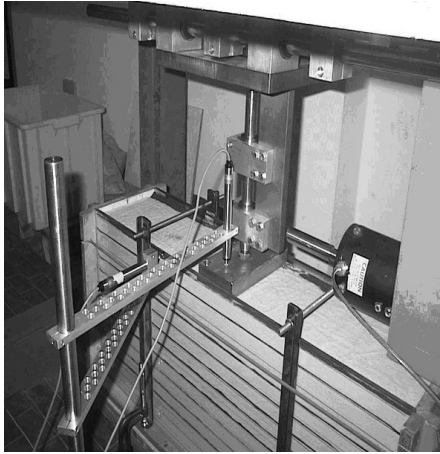


Figure 1: The loading device and the experimental setup

### 2.3 Design of the photogrammetric survey

In order to acquire more accurate information about the displacement field under the foundation, a digital camera has been placed in quasi-nadir position with respect to one of the glass walls, recording images at a rate allowing to describe the phenomenon until the collapse of the sand.

Because of the test setup, the displacement field can be considered as plane (and symmetrical with respect to the vertical plane normal to the glass and passing through the foundation centre). This allows to apply a image rectification to convert image displacement into object displacements, with the additional advantage of a simpler setup (a single camera, no synchronization required).

To compute the 8 parameters of the transformation for every image of the sequence and to establish a permanent reference system to make comparisons, a polyester frame has been placed on the outer side of the glass, covering the area interested by the displacements (20x30cm). A set of 32 calibration targets, whose position is known with an accuracy of about 0.01 mm has been printed on it (see Figure 2). Computation of the parameters for each image of the sequence would be redundant if the arrangement camera-device is perfectly stable during the test; unfortunately, this turned out not to be true after the first experimental trials, which revealed small movements of the camera, most probably due to vibrations caused by the compressor needed to operate the oleo-dynamic actuators.

In principle, the transformation parameters computed using points on the reference frame should not be applied to points of the sand layer on the opposite side of the glass wall, because they lay on a different plane. However, the total displacement of a point during the test is just of a few mm and only displacements, and not absolute coordinates, must be measured precisely. Therefore the error coming from ignoring refraction through the glass and applying the rectification parameters to a different plane has been neglected. By a similar reasoning, also lens distortion has been neglected, since its variation along the image displacement of a point is very small.

A Kodak DCS420 with a CCD array of 1524 by 1012 pixels (square pixels with 9  $\mu\text{m}$  size) has been fitted with a 24 mm lens. Because each loading test lasts 15-30 minutes, an external electronic trigger has been connected to the camera in order to control image acquisition at fixed steps, synchronized to transducers and other sensors for comparison. The frequency of acquisitions depends on the speed of displacement in sand; for

tests described below, four images per minute have been taken, even though only a subset of these has been processed.

The camera is placed on a tripod at a distance of about 50 cm from the glass wall, resulting in a mean pixel-size in object space of about 0.2 mm.

As shown in the following, after an initial setup for the test, the measurement proceeds automatically, driven by image matching algorithms. The extraction and measurement of calibration targets is carried out by l.s. template matching, being a priori known the shape of each target to be measured in all images. Tracing of sand's surface displacements consists in finding the same homologous points in all the image sequence. Because of their size and of movements induced by the stress (that lead to a certain mixing, rearranging and rotating them) neither individual grains nor cluster of them can be traced. Several small white spheres have therefore been positioned as tracing points in the sand near the glass wall, at the nodes of a grid (see figure 2). Weight and diameter of spheres has been selected to let unmodified the mechanical behaviour of sand, while their colour contrasted enough to guarantee identification against the background.

Although preparation of the specimen is not a simple and fast matter (some hours for each loading test are needed), this solution yields a high resolution description of the displacement field. This advantage is very important for the geotechnical analysis, where investigation of initial loading steps is the most interesting issue. Because at this stage displacement are very small, the accuracy required is in the order of 0.1 mm at object scale.



Figure 2: The reference frame and the area of the specimen interested by displacements (about 30x20 cm), before and after loading (test 1).

### 2.4 Processing of a test image sequence

Once a test has been completed, images are downloaded from the camera memory to a PC. The quality of the colour images is generally not very good with this camera, but no pre-processing stages are needed, apart image format and colour to grey value conversion. Although the sand texture and colour does not offer a well contrasted background and some grains are highly reflective, illumination and exposure could be adjusted in such

a way as to have spheres sufficiently discriminated against the sand.

To control the automatic tracing procedure, the user is required to setup the parameters of the matching algorithm and to carry out some initial manual measurements, i.e. the localization and labelling of the position of the spheres as well as the measurement of the approximate position of at least two calibration targets in the first image. Position of the other fiducials in the same image can be derived by a simple conformal transformation, because their position in the frame reference system is known. As initial matching location in the following images, the same value assumed for the first image can be used for the calibration targets; even if the camera is not perfectly stable during the test, its displacements are very small and approximations still hold.

Tracing the spheres along the image sequence is made up of the following items, which are applied to each image:

1. sub-pixel measurement of calibration targets;
2. computation of image rectification parameters;
3. prediction of the sphere location in the next image based on its position in the current image;
4. computation of object coordinates for all spheres by applying the parameters.

Image measurement is performed by *least squares matching* (Gruen, 1985; 1996), with an affine transformation which may compensate also for rotations and scale variations of corresponding points. The reason for using the affine model is that the spheres can be partially covered by sand grains, so that allowing rotations improves the fit; besides, it happens sometimes that a sphere is pushed away from the wall inside the sand, so allowing a global scale variation again improves the fit. No radiometric correction is implemented in the l.s. matching algorithm, but mean and variances of template and patch are equalized prior to the matching (Baltasvias, 1991).

The measurement of fiducials on the frame is performed by template matching with a synthetic copy of the target. For the tracing points, the template is a square window resampled around the sphere location in the previous image; the centre of this window is used as initial location of the patch in the second image. This solution works fine as far as displacements are small, as it happens at the beginning of the loading cycle, but later the movement lead to displacements in image space larger than the convergence radius, so that matching would fail. Modelling as a time dependent function this displacement would allow to predict the homologous point position on the basis of its previous path could be computed, as shown in the next section. Here we followed a simpler approach, which exploits the fact that the largest component of the sphere displacement is along vertical lines, so that other initial positions can be set up along this direction at pre-fixed steps.

This method allows to trace all spheres along the image sequence, barring a little fraction which are lost in the last stages of the loading. However, overall, this failures did not compromise the evaluation of the displacement field. Possible cause of failure in tracing may be the disappearing of a sphere into the sand, disturbances introduced by reflections on the glass or large displacements which cannot be traced with the simple prediction model.

Since the acquisition time of each image is recorded, not only the displacement field, but also the velocity field can be computed.

As far image measurement accuracy is concerned, the l.s. matching figures are about 1/20 the pixel size, resulting in about 0.45  $\mu\text{m}$ .

## 2.5 Results of experimental tests

The first experimental loading test concerned a sand featuring a quite low relative density (incoherent material). In Table 3 some characteristics of this trial have been summarized, with the indication of the number of successfully traced points in the whole sequence.

Trial	# of spheres	# of traced spheres	# of images	frame rate (s)
1	190	175	77	30
2	102	98	40	30

Table 3: features of experimental tests

To independently check the results, both diagrams time-displacement of the points just below the foundation, evaluated by photogrammetry and by the strain gauge measurement have been compared. While it is apparent that they show the same behaviour, a metric evaluation is not possible, because the two methods do not determine the displacements of the same points. Thus the measurement accuracy of tracing points has been estimated indirectly, by comparison with the accuracy of fiducials. By considering a few fiducials as control points and looking at the discrepancies between estimated and known coordinates of the remaining, an accuracy in object space of about 15  $\mu\text{m}$  has been estimated. To derive the accuracy of the sphere, where we don't have any independent control, by analogy we assumed that of the fiducials, reduced by the ratio of the average values of the correlation coefficients obtained by the l.s. matching process for both kinds of points. The estimated value turns out to be about 18  $\mu\text{m}$ , largely inferior to the required value of 0.1 mm.

Figure 4 shows the whole displacement field, plotted with the program GID ([gid.cimne.upc.es](http://gid.cimne.upc.es)).

In a second loading test, the device was filled with sand of mean density. During this trial a sudden variation in load intensity was applied to check the sensibility of the method. In the diagram time-load reported in Figure 6, a small load reduction (from point A to B) was followed by an increment of 20 kg applied (point C) in 5 s. At the end of this blip, it can be seen that the original curve has been recovered. The selection of a higher sampling rate of the sequence (30 s) permitted to accurately follow the displacements.

Figure 5 shows another kind of visualization of the displacement field obtained by GID software; in this case, a mesh representation of tracing points at two different stages of the trial is given. Apart from visualization purposes, the mesh structure is very important as pre-processing step for the *finite-element* analyses.

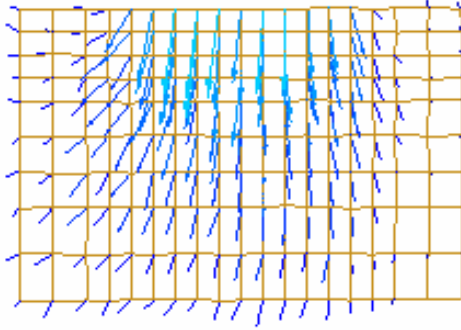


Figure 4: Visualization of tracing point vector displacements (magnitude x10) after 1220 s from the beginning of loading (test 1)

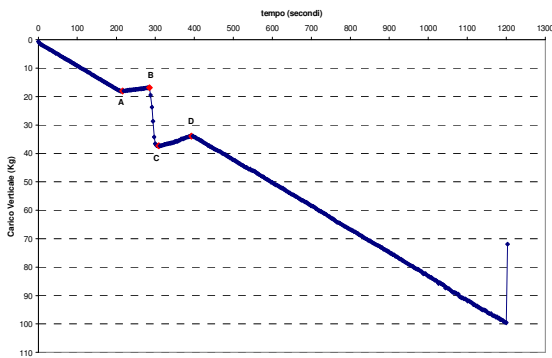


Figure 5: diagram time-load for test 2, showing a sudden variation of loading.

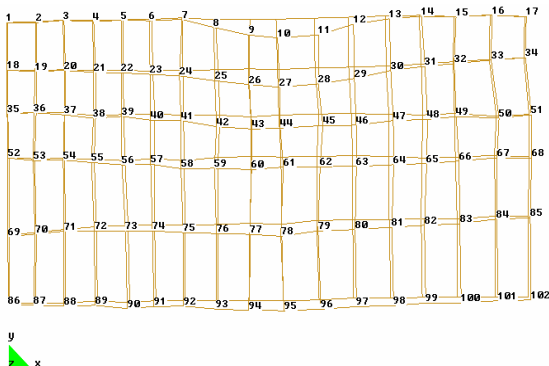


Figure 6: Mesh representation of the tracing point positions in image 1 and image 11 (test 2)

### 3. TRACKING THE DISPLACEMENT OF POINTS ON A SLIDING SURFACE

#### 3.1 Test goal and test setup

In a second application, the goal was to track the movement of points on the superficial layer of a sand specimen, sliding along a sloping plane. As in the previous case, the goal was to compare the actual dynamic of the grains with the prediction of a mathematical model. This is of interest in trying to model the conditions that lead to landslide in this kind of terrains. The experiment was carried out in a channel about 4 m long and 50 cm wide with a sand height of about 15 cm (fig. 7). The specimen is arranged in the sloping side of the channel and kept

in place by a gate. The specimen can be prepared with different sand types, with varying humidity contents, while the testing device can vary the inclination of the upper channel section to reproduce different slope angles.

The release of the gate set the sand specimen sliding, until the slope change of the channel slow down and then stops the movement; the motion of the superficial layer of sand should be traced.

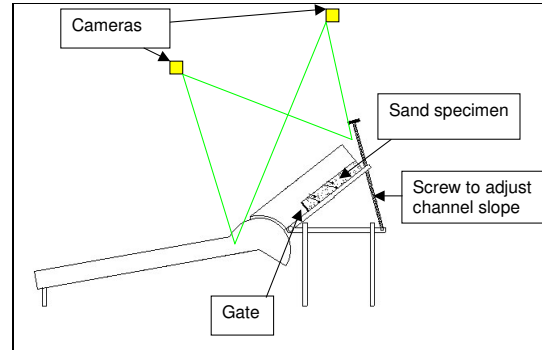


Figure 7: the testing channel and the camera's locations

As in the previous experiment, tracking individual sand grains is not possible, so we resorted to spheres. Due to the test dynamics, we had to ensure that they were faithfully following the sand movement and that they could be traced against the sand background. To this aim, pins were fixed to the spheres and tests were carried out with different pin length and sphere size. Though this solution may not be optimal (some pin get out of the sand and starts rolling, becoming useless to describe the sand movement) visual examination of different tests confirmed that the sphere actually follow the sand quite closely.

To ensure a dense description of the surface deformation, a grid of 12x16 spheres, spaced about 3 cm was prepared and put in place with drilled board, to guarantee precise positioning of each sphere in the channel reference system in every trial. The position of the targets in object space and their labels are therefore known as long as the gate is closed.

Being the displacement field 3D, two synchronized digital cameras Basler AF 101 (1300x1000 resolution, focal length 8 mm, pixel size 6.7 micrometers, 12 fps at full resolution) were employed to track the trajectories. In order to raise the frame rate of the camera, we took advantage of the elongated shape of the channel, using just half frame. We could therefore achieve 22 fps, which proved just enough to capture the motion.

The cameras were mounted with convergent axes over the channel, covering the section where the movement actually take place, about 1.8 m long. The camera are mounted about 1.4m above the specimen, with axes are convergent to the centre of the channel section and a base/distance ratio close to 1. With this arrangement, assuming a measurement accuracy of 1 pixel, a simulation of the spatial intersection from the cameras predicted an accuracy for the sphere positions of 3 mm in horizontal and 5 mm on Z.

A reference frame was established on the channel by fixing 40 targets along the top of the walls and before the gate, on the channel bottom. Their coordinates were determined photogrammetrically within a block adjustment of 8 convergent images taken with a Nikon D100 with a 18 mm lens, yielding an estimated accuracy of 0.5 mm in all directions.

### 3.2 Tracking strategy

To track the spheres along their trajectory and compute the coordinates at each frame, the following strategy has been implemented:

- a) target extraction by an interest operator, in each image;
- b) labelling of each target in each frame;
- c) computation of object coordinates by spatial intersection of the homologous rays.

### 3.3 Target extraction

In each image, the spheres are extracted in two stages: first the Foerstner operator is applied to extract (possibly only) all tracing points, then the interest points are filtered by template l.s.m. using a synthetic image of the sphere to reject false candidates.

Indeed, it proved difficult to achieve to the above mentioned goal. Due to the high reflectance of the sand grains, the spot of grain were often as “interesting” as a nearby sphere. This make obviously more difficult to discriminate, when labelling the targets. On the other hand, the illumination level was kept high, to allow shorter shutter time. Some improvement was obtained spraying ink over the sand surface, so reducing the spot intensity. Trying to discriminate based on the roundness of the interest point didn't yield the expected results, so we had to accept as potential targets many more candidates than the number of spheres, in the hope that filtering by l.s.m. would discard the false targets. This was partially successful, because we had to allow for scale and shape parameters in the matching, due to variations of image scale and reflection spots on the spheres. Overall, with some tuning of the options in feature extraction and l.s.m., we could find values all right in every test, with the same illumination, but still we ended up with more interest points than targets. Figure 8 shows two images of the sequence just after releasing the gate. Depending on the slope angle, it may happen that the last column of spheres remain still.

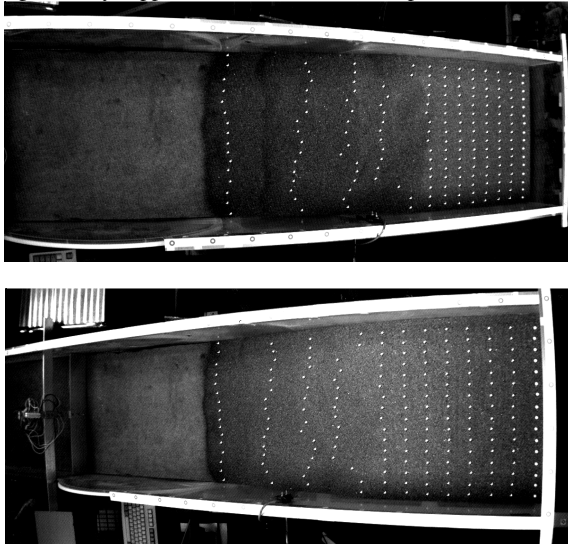


Figure 8: Left and right view of a test sequence.

### 3.4 Labelling of the targets

To consistently track the spheres along their trajectory, it was decided to estimate a polynomial function for each sphere, to predict its position in subsequent frame. The position in image

space depends on the movement of each sphere and on the radial distortion, which reaches 400 micrometers and more at the image border and must therefore be accounted for.

As a compromise between a too simple linear model and a more accurate model with linear changes of acceleration, we used a 2<sup>nd</sup> order polynomial, whose coefficients can be estimated from the position of the same target at three epochs. Sudden changes in speed and direction of the sand occur during the sliding of the specimen. This risks sometimes to render the prediction of the position inaccurate, because the frame rate is too low. An obvious solution to this problem would be increasing it, but we could not reduce image resolution to this aim, because we would have missed too many targets in such case.

To start the prediction, the operator selects and labels 6 targets on the first image of the sequence. Since the specimen surface is planar, the approximate position of the other targets in the image is computed by a rectification from object to image plane, using the object point coordinates of the board drills.

The labelling of the 2<sup>nd</sup> and 3<sup>rd</sup> image targets is performed by naming the candidate closest to the position in image 1<sup>st</sup> in positive x direction, i.e. along the channel: since the displacement in the first images applies only to the first columns and is still small compare to the column spacing, this works fine.

In the subsequent images, the position of each target in the next image is predicted. Then the closest candidate to that position is found and assigned the label and the coefficient of the prediction model are updated with the new position.

A series of checks was therefore set up to discriminate ambiguities and to deal with the spheres starting to roll faster than the sand because the pin, due to differential movements of the sand layers, came to the surface, becoming ineffective.

### 3.5 Computation of object coordinates

After each frame sequence for a single camera has been processed, yielding the pixel coordinates of each sphere in the sequence, coupling of the homologous spheres along the sequence is performed exploiting the epipolar geometry, after space resection of the camera stations and attitudes from the control point coordinates. The theoretical accuracy of the targets in object space is the same predicted by the simulation (RMS of 1.2 mm in X,Y and of 2.5 mm in Z). This means about 1 pixel accuracy in object space which is not really much for target and images of good contrast, although well within the specification of the experiment. Since the coordinates are computed with a direct formula for space intersection, the parallax in object space is available and can be used to check whether the labelling is correct.

### 3.6 Results

A series of 4 tests have been executed with different slope angles and different sand quality. Overall, the procedure is successful as far as the slope angle is not too high: in such cases, too many pins get out of the sand and also, because of higher dynamics, the prediction model fails more often.

Apart from the initial labelling of 6 points in the first image, the procedure of selection, tracking, labelling and point coupling runs automatically.

With medium and low slope angles, on average about 95% of the 176 targets were traced along the sequence in every test, despite a rather low frame rate. Parallaxes in object space are normally between 0.1 and 0.8 mm; suddenly, if the prediction fails, they increase by one or more order of magnitude, so the

target is rejected from the sequence (see the abnormal position and velocity vector in Fig. 9, at the bottom).

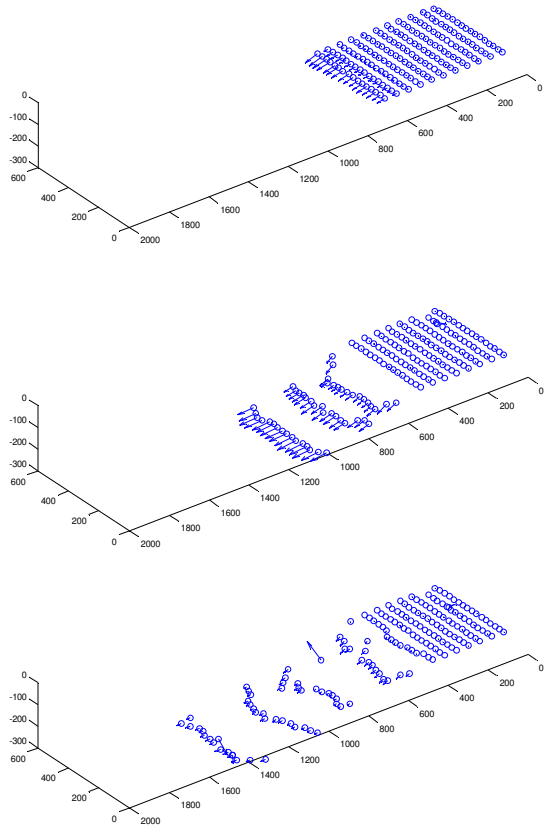


Figure 9: 3D position and velocity vectors of the targets at different times

In order to assess the repeatability of the test under identical condition, the trajectories of target 79 (2nd column, middle) in four test have been superimposed on the same graph (see Fig. 10 and 11).

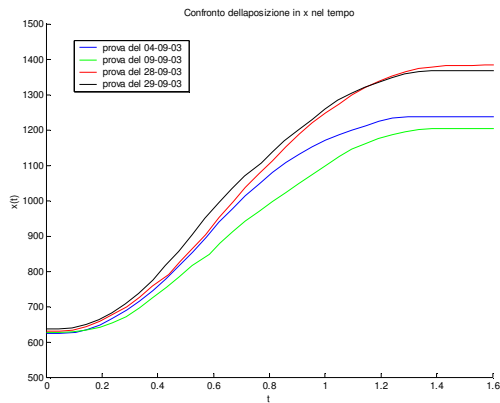


Figure 10: position of the target 79 at different times

It can be seen that the agreement is quite good, especially for velocities (the differences in the final position are up to 20 cm,

this depends on a different height of the sand specimen in these tests).

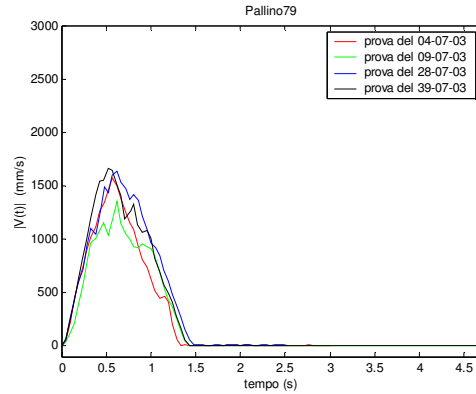


Figure 10: position of the target 79 at different times

#### 4. CONCLUSIONS

Overall, both cases were solved to a high degree of automation, and with accuracy level that, perhaps of not-so-high quality in the second case, but still more than enough for the application at hand. Using a prediction model to label the target along the sequence seems to be a feasible and flexible technique, but its reliability with only two cameras and a low frame rate cannot be guaranteed and demands additional efforts to control the results.

#### References

Montrasio, L., and Nova, R., 1989. Assestamenti di una fondazione modello sotto carico inclinato: risultati sperimentali e modellazione matematica, *Rivista Italiana di Geotecnica*, pp.35-49.

Hampel, U., and Maas, H.-G., 2003. Application of Digital Photogrammetry for Measuring Deformation and Cracks during Load Tests in Civil Engineering Material Testing. In *Proc. of Optical 3D Meas. Tech. VI*, Zurich, pp. 80-88.

Gruen, A., 1985. Adaptive least squares correlation: a powerful image matching technique. *South African Journal of Photog., Remote Sensing and Cartography*, 14(3), pp. 175-187.

Gruen, A., 1996. Least squares matching: a fundamental measurement algorithm. In: K. Atkinson (ed.), *Close Range Photogrammetry & Machine Vision*, Whittles, pp. 217-255.

Baltsavias, E.P., (1991). *Geometrically Constrained Multiphoto Matching*. Mitteilungen No. 49, Inst. of Geodesy and Photogrammetry, ETH, Zurich.

Gordon, S.J., Lichti, D.D., Chandler, I., Stewart, M.P., Franke, J., 2003. Precision Measurement of Structural Deformation using Terrestrial Laser Scanners. In *Proc. of Optical 3D Measurement Techniques VI*, Zurich, pp. 322-329.

#### References from websites

[www.cimne.upc.es](http://www.cimne.upc.es), accessed at 1 May 2004.